Buckling instability of lipid tubules with multibilayer walls under local radial indentation

Yue Zhao, Linan An, and Jiyu Fang*

Department of Mechanical, Materials, and Aerospace Engineering, Advanced Materials Processing and Analysis Center, University of Central Florida, Orlando, Florida 32816, USA

(Received 4 April 2009; published 13 August 2009)

The mechanical behavior of self-assembled lipid tubules is an important property which determines their suitability for technological applications. We study the instability of multibilayer lipid tubules (with wall thickness t and external radius R_{ext}) beyond elastic response under local radial atomic force microscopy indentations. A discontinuity in force-distance curves associated with the buckling instability of lipid tubules is observed. The critical force at which lipid tubules undergo a buckling transition linearly scales as t/R_{ext}. In addition, a reduced critical buckling force is found to extend a distance of ~ 1 μm from the end of lipid tubules.

DOI: 10.1103/PhysRevE.80.021911 PACS number(s): 87.15.La, 87.15.A−, 87.64.Dz

I. INTRODUCTION

Self-assembled lipid tubules with crystalline bilayer walls have raised considerable interest due to their potential uses as organized templates for protein crystallization [1,2] and metallization [3–7], controlled release systems for drug delivery [8–10], and encapsulates for functional molecules [11–14]. During the past decade, much progress has been made in understanding the structure, morphology, and molecular ordering of lipid tubules [15–21]. The self-assembly mechanism of lipid tubules has also received considerable attention from a theoretical point of view [22–26].

The mechanical behavior of lipid tubules is an important property for many of their applications. There have been attempts in measuring the mechanical properties of lipid tubules by bending them with optical tweezers [27] and moving contact lines [28,29]. However, these bending experiments probe the mechanical properties of lipid tubules over a large length scale. Atomic force microscope (AFM) is emerging as a powerful nanoindentation tool for studying the elastic properties of individual supramolecular assemblies, including lipid vesicles [30,31], virus capsids [32–35], and protein tubes [36–41], by the measurement of force-distance curves when the AFM tip moves up and down over a point on their surfaces. The Young's modulus of individual supramolecular assemblies can be determined by the analysis of the force-distance curves with appropriate theoretical models. We have studied the radial elasticity of self-assembled lipid tubules of 1,2-bis(tricosa-10,12-diynoyl)-*sn*-glycero-3-phosphocholine ($DC_{8,9}PC$) by AFM indentation [42]. The linear elastic response of the lipid tubules subject to small loading forces is well described by the finite element method, giving a Young's modulus of ~703 MPa. One of the advantages of AFM indentation is its better control over loading forces. Therefore, a greater range of loading forces can be applied on lipid tubules to understand their structural instability under large deformation. In this paper, we report the buckling instability of lipid tubules with multiple-bilayer walls beyond linear response under local radial AFM indentations. The critical force at which lipid tubules undergo a buckling transition linearly scales as t/R_{ext}, where t is the wall thickness and R_{ext} is the external radius of lipid tubules. Furthermore, we observe a reduced critical buckling force near the tubule ends.

II. EXPERIMENTAL METHODS

Lipid tubules were synthesized by thermal cycling of a 5 mg/mL suspension of 1,2-bis(tricosa-10,12-diynoyl)-*sn*-glycero-3-phosphocholine ($DC_{8,9}PC$) (Avanti Polar Lipids, Alabaster, AL) in ethanol/water (70:30 v/v) from 60 °C to room temperature at a rate of ~0.5 °C/min [43]. The polymerization of lipid tubules in solution was performed with a UV light (254 nm) for 20 min at room temperature. AFM (Digital Instruments Dimension 3100) with software version 6.12r1 was used to study the structure and mechanical properties of lipid tubules in an open liquid cell. Silicon nitride cantilevers (Nanosensors) were employed. The size of the cantilever tips (radius of curvature) is about 15 nm according to the manufacturer. Indentation experiments of lipid tubules were conducted in contact mode at room temperature. Force-distance curves were recorded by measuring the deflection (force) of the cantilevers as they approached the lipid tubules.

The Young's modulus was calculated from the measured stiffness of lipid tubules with the finite element analysis. In the finite element simulation process, lipid tubules were modeled as tubes made of a homogeneous material and loaded by a rigid spherical indenter with a radius of 15 nm, similar to the size of AFM tips used in our indentation experiments. Considering axial symmetry of the problem, the model was reduced to a quarter sector using the two mirror-symmetry planes intersecting at the loading point. This quarter sector was divided into 4500 brick elements and subjected to axisymmetrical boundary conditions. The Poisson ratio of lipid tubules was chosen as 0.48, the mean value of common biomaterials. The post processing was done by the commercially available ABAQUS 6.6 program. ABAQUS is designed for the finite element analysis of the behavior of solids and structures under loading. In our experiments, loading was simulated by prescribing a downward movement of the

*jfang@mail.ucf.edu

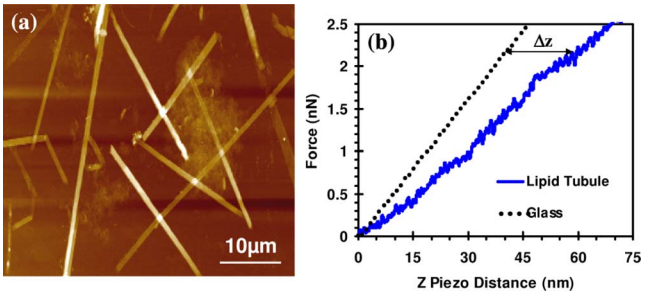

FIG. 1. (Color online) (a) Contact mode AFM image of lipid tubules adsorbed on a glass substrate. The image was taken in a liquid cell at room temperature. (b) (FZ) piezodistance curve (solid blue line) on an intact lipid tubule with an external radius of ~250 nm under a maximum loading force of 2.5 nN, together with the FZ curve (dotted dark line) on a glass substrate. Both FZ curves were performed in a liquid cell with the same AFM tip during the approach process and shifted along the z-distance axis to set the tip-sample contact point to zero. The horizontal difference ΔZ between the two curves for a given loading force represents the indentation depth of the lipid tubule by the AFM tip.

rigid spherical indenter, which was calculated in increments of 100. The AFM tip-lipid tubule contact was modeled as frictionless. The Young's modulus and wall thickness of the modeled tubules were adjusted and the analysis was repeated until the measured stiffness of the modeled tubules fitted the measured stiffness of the lipid tubules.

III. RESULTS AND DISCUSSION

In our experiments, a drop (~100 μl) of $DC_{8,9}PC$ tubule solution was placed onto a clean glass slide and left to dry for 30 min in air at room temperature. A drop of water was then added onto the tubule-adsorbed glass substrate to ensure a complete immersion of an AFM cantilever in an open liquid cell. All tubules were adsorbed on the glass surface, as evidenced from the low-resolution AFM image shown in Fig. 1(a). The image was taken in contact mode at a scanning rate of 0.5 Hz and a 512×512 pixel size. Most of the adsorbed tubules were intact and showed cylindrical shapes, suggesting that they were not grossly distorted during the sample preparation. The measured height of the intact tubules was 500 ± 10 nm, which agrees with the diameter of lipid tubules measured by electron microscope.

To position an AFM tip in the center region of an intact lipid tubule, we set the long axial of the AFM cantilever to be parallel to the long axis of the tubule by rotating the sample under the guidance of the optical microscope built in the AFM. To minimize the effect of thermal drift on the indentation positions, we gradually reduced the scan size after locating an intact tubule at a slow scanning speed of 0.3 μm/s in a large size of view. We then tuned the tip position by making a profile scan and redirecting the tip to the middle of the cross section of the tubule before beginning the indentation experiments. The force-z (FZ) piezodistance curves were recorded as the AFM tip approached the tubule. Since the AFM cantilever is at an angle relative to a sample surface, plowing can occur due to the X movement caused by coupling of the Z and X axes of the piezoscanner during indentation. When indenting in the Z direction, the X-rotate parameter allows us to add a movement of the scanner opposite to the direction in which the cantilever points. In our experiments, the X-rotate parameter was set to 22° to prevent the AFM cantilever from plowing the surface along the X direction. Figure 1(b) is a typical FZ curve taken on an intact lipid tubule with a uniform external radius of ~250 nm at a speed of 600 nm/s with a maximum loading force of 2.5 nN, together with the corresponding cantilever deflection curve on a glass substrate, which can be considered as an infinitely stiff material compared to AFM cantilevers. Both FZ curves, which were taken with the same cantilever during the approach process, were shifted along the Z-distance axis to set the tip-sample contact point to zero. The horizontal difference between the Z distance of the lipid tubule and the cantilever deflection for a given loading force is the indentation (ΔZ). As can be seen from Fig. 1(b), once contact is established, a linear response is observed in the FZ curve. The linear FZ curve is highly reproducible during the repeated indentations under the loading force of 2.5 nN. At this loading force, the tubule is indented by ~23 nm. The retraction FZ curve under this indentation condition shows only a very small hysteresis. After repeated indentations in the linear regime, the tubule is reimaged by AFM. We observe no evidence of collapse and damage, suggesting that the tubule undergoes elastic deformation. The spring constant measured from the slopes of the linear FZ curves taken from 52 intact tubules with an external radius of ~250 nm is 0.036 ± 0.002 N/m.

To probe the structural instability of lipid tubules beyond their elastic response under radial AFM indentations, we increased loading forces. Figure 2(a) shows the FZ curves taken by three repeated indentations at a speed of 600 nm/s with a maximum loading force of 5 nN. We find that the initial linear response for the first indentation persists up to a critical loading force of 3.6 nN. At this point, there is a sharp drop in force. The indentation at this point is ~72 nm, corresponding to ~14% of its origin height. The force then increases with further indentation. The discontinuity of FZ curves was also observed in the AFM indentation experiments of virus capsids [32,35,44,45] and protein microtubules [36,40]. It was considered as an indicator of the buckling or failure of shell structures. The subsequent AFM image taken immediately after the sharp drop in force shows that the tubule undergoes a buckling transition from convex [Figs. 2(b) and 2(c)] to concave curvature [Figs. 2(d) and 2(e)]. The buckling transition of lipid tubules can be viewed as a localized, nonlinear instability [46]. The height profile in Fig. 2(e) shows that the depression is ~80 nm, which is slightly larger than the indentation (~72 nm) measured from the FZ curves. The sharp drop in force observed in the first FZ curve [Fig. 2(a)] is likely due to the buckling of the tubule wall away from the end of the AFM tip. After buckling, the FZ curve cannot be retraced when the AFM tip is withdrawn from the tubule surface at the speed of 600 nm/s. There is a large hysteresis in the retraction FZ curve. However, the buckled tubule can recover its original convex curvature after relaxation for 10 min in water at room temperature [Figs. 2(f) and 2(g)]. By repeatedly taking the FZ curves

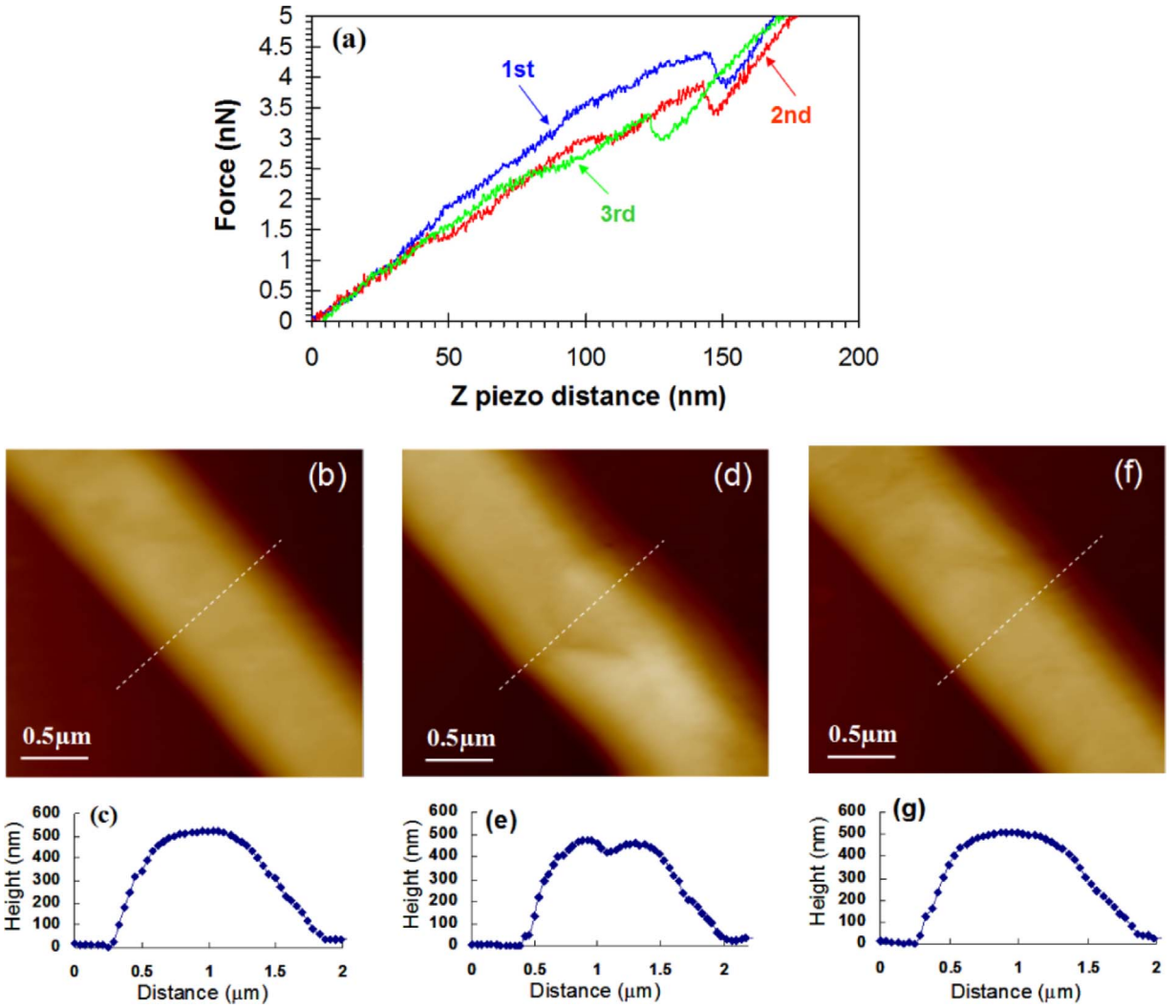

FIG. 2. (Color online) (a) FZ piezodistance curves of three repeated indentations on an intact lipid tubule with an external radius of ~250 nm under a maximum loading force of 5 nN. These FZ curves were taken 10 min apart. (b) AFM image taken before the indentation. (c) Height profile along the dashed line shown in (b). (d) AFM image taken after the first indentation. (e) Height profile along the dashed line shown in (d). (f) AFM image taken after 10 min relaxation in water at room temperature. (g) Height profile along the dashed line shown in (f).

on the same region of the recovered tubule after each 10 min relaxation with the same loading speed and loading force, we find that the recovered tubule shows a slight softening as evidence of the decrease in the slope of the second and third FZ curves [Fig. 2(a)]. The softening under the second and third indentations was observed for all tubules tested. The critical buckling force F_{crit} at which the tubule undergoes the buckling transition decreased from 4.2 to 3.4 nN after three indentations [Fig. 2(a)], suggesting that the tubule is not fully recovered in terms of its mechanical strength after 10 min relaxation. Presumably, the lipid molecules rearrange in the tubule walls after buckling. However, the resolution of the AFM image of the recovered tubule shown in Fig. 2(f) is not sufficiently high to examine the possible rearrangement.

Furthermore, we perform a series of indentations from the end of a lipid tubule to the middle section [Fig. 3(a)] with the same AFM tip at the same loading speed and loading force. Since there is a slight decrease in the F_{crit} for the second and third FZ curves [Fig. 2(a)], we use the first forward FZ curve of each indentation to determine the F_{crit} near the end of the tubule. Figure 3(b) is a plot of the F_{crit} as a function of the distance along the longitudinal direction. It is known that the sudden drop in force may also be a result of the tip slipping off the top surface of a tubule during indentation. The data shown in Fig. 3(b) were taken after the buckling was confirmed by reimaging. Exact determination of the indentation position along the tubule longitudinal direction is difficult due to thermal drift. In our experiments, the thermal drift of the AFM indentation was estimated to be less than 20 nm (<4% of the tubule diameter) by imaging a lipid tubule adsorbed on a glass substrate over time at a scanning speed of 0.3 μm/s [42]. Thus, we conclude that the uncertainty of measuring the indentation positions along the longitudinal direction is less than 20 nm. As can be seen in Fig. 3(b), the F_{crit} reduces from 4.5 to 4.1 nN over a distance of ~1 μm from the tubule end. The reduced F_{crit} near the tubule ends is also observed when a series of indentations is carried from the middle of a lipid tubule to the end. Recently, we studied

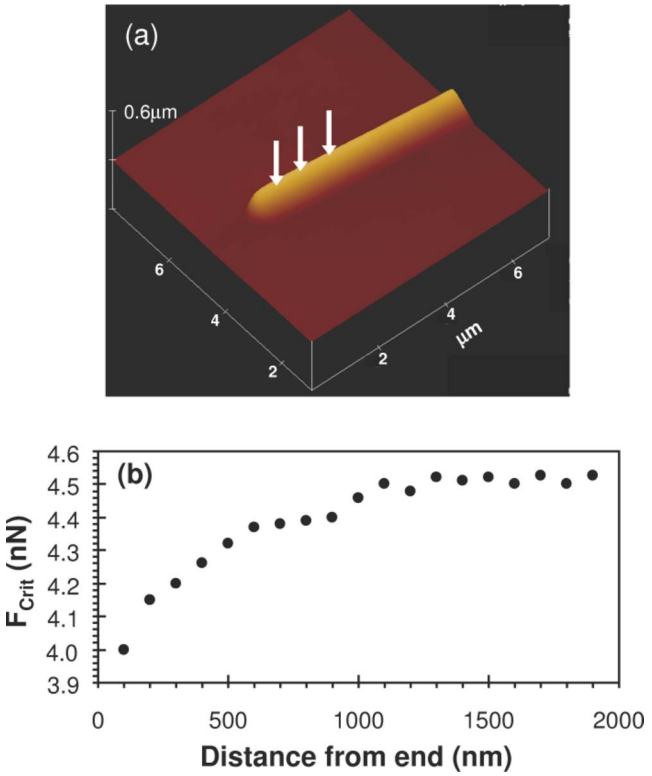

FIG. 3. (Color online) (a) Contact mode AFM image of a lipid tubule adsorbed on a glass substrate. This image was taken before the indentation. One end of the lipid tubule with a uniform radius of ~250 nm is visible. (b) Critical buckling force F_{crit} at which the tubule undergoes a buckling transition as a function of distance from the tubule end. The F_{crit} was measured from the first forward FZ curve of each indentation along the long axis of the tubule shown in (a).

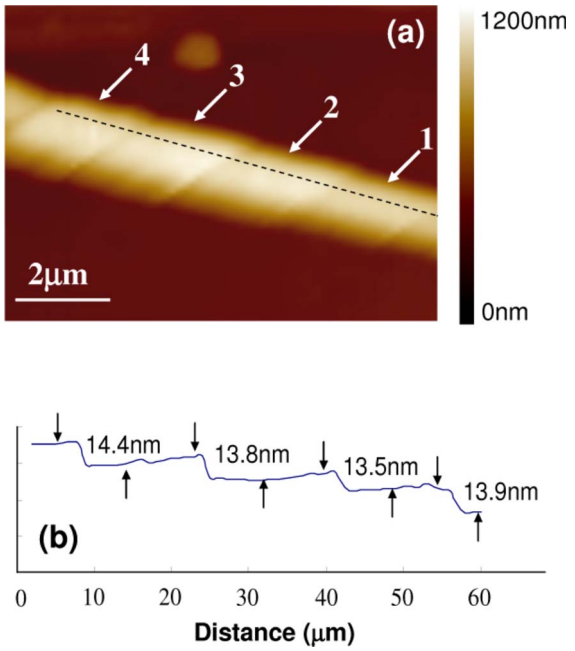

FIG. 4. (Color online) (a) Contact mode AFM image of a cigarlike tubule with helical bilayer edges on its surface. (b) The height profile along the dashed line shown in a, showing the four step edges on the tubule surface. Each step corresponds to two-bilayer increase.

the diffusion of Nile red (NR) in the crystalline bilayer walls of $DC_{8,9}PC$ tubules with the fluorescence recovery after photobleaching (FRAP) and found that the FRAP kinetics of NR showed a distinct position dependence. The diffusion of NR slowed down at the middle of a lipid tubule while it became faster at its ends [47]. This result indicates that the packing density of lipid molecules near the tubule ends is lower than that in the middle. So we conclude that the variation of lipid packing in tubule walls leads to the reduced F_{crit} near the ends of lipid tubules.

Based on how a bilayer sheet warps around the tubule core, different morphologies of lipid tubules can be formed. The rolling up of a wide planar bilayer sheet around a corner can lead to the formation of a cigarlike tubule in which the edges of bilayer sheets appear on its external surface as helical markings. For the lipid tubules formed in ethanol/water solution, a small number of cigarlike tubules are observed by AFM [Fig. 4(a)]. The apparent width of the cigarlike tubule is broadened by the finite size of the AFM tip. In our experiments, the external radius (R_{ext}) of lipid tubules was determined by measuring their heights. The height profiles across the cigarlike tubule reveal that the R_{ext} of four sections marked in Fig. 4(a) are ~290.5, ~275.7, ~266.1, and ~248.4 nm, respectively (see Table I). The height profile along the long axis of the cigarlike tubule reveals four step edges [Fig. 4(b)]. The measured thicknesses of these steps are 14.4, 13.8, 13.5, and 13.9 nm, respectively. This suggests that each step increases by two bilayers because the thickness of single bilayers in tubule walls determined by x-ray diffraction from $DC_{8,9}PC$ tubules is ~6.6 nm [17]. By comparing the measured height of each section (Table I), we conclude that the increased R_{ext} of the sections along the long axis is mainly a result of the increase in the number of lipid bilayers (e.g., the internal radius R_{int} is approximately constant, while the R_{ext} is proportional to the number of lipid bilayers).

The cigarlike tubule provides a simple system to study how the mechanical property of lipid tubules is associated with their morphologies. Since there is a slight softening of lipid tubules for the second and third FZ curves [Fig. 2(a)], we use the linear part of the first forward FZ curve to determine the spring constant of each section. The tubule and cantilever system are considered as two harmonic springs arranged in a series. The point spring constant (stiffness) of each section is calculated according to the equation $k_{tub} = \frac{k_{can}k_{mea}}{k_{can}-k_{mea}}$ (Hooke's law), where the measured spring constant (k_{mea}) is the slope of the first FZ curve and k_{mea} is the spring constant of the cantilever, determined to be ~0.051 N/m by measuring its thermal fluctuations [48]. The calculated k_{mea} of each section are given in Table I.

The Young's modulus E of each section can be estimated from the measured k_{tub} with the finite element analysis. Since the FZ curves of multibilayer lipid tubules under the loading speed of 600 nm/s show a considerable similarity to that of single layer virus capsids [32,35] and protein microtubules [36,40], it is reasonable to suggest that there is no sliding

TABLE I. Summary of calculated external radius (R_{ext}), wall thickness (t), spring constant (K_{tub}), critical buckling force (F_{crit}), and Young's modulus (E) of each section of the tubule shown in Fig. 4(a).

Section	R_{ext} (nm)	K_{tub} (N/m)	t (nm)	E (MPa)	F_{crit} (nN)
1	248.4	0.029	24.4	1440	3.6
2	266.1	0.039	39.6	960	3.8
3	275.7	0.049	52.8	715	4.2
4	290.5	0.058	66.0	610	4.3

between the lipid bilayers within tubular walls. In this framework, the multibilayer tubules were treated as single-layer elastic shells made from a homogeneous material with the R_{ext} shown in Table I. The contact between the AFM tip and the tubule was modeled as frictionless. Figure 5(a) shows the deformed shape of a half segment of a tubule under AFM indentation. The distribution of the von Mises stress coded by color can be clearly seen in the zooming image at the contact point. We note that the deformed region of the modeled tubule extends for ~30 nm from the contact point, which is smaller than the deformed region of the buckled tube [Fig. 2(e)]. In the finite element simulation, AFM tips were modeled as a spherical indenter with a radius of 15 nm. However, the AFM tip used in our experiments has a pyramidal geometry with the curvature radius of ~15 nm. We expect that the side of the pyramidal tip will contact with tubule walls when the indentation is larger than 15 nm. The side contact may lead to the large extension of the deformed region observed in our experiments. The finite element model allows us to follow the deformation of a tubule as it is indented. During the simulation, we varied both E and t until the simulated force-indentation curve was best fitted with the measured k_{tub} of the tubule [Fig. 5(b)]. The optimally fitted results of E and t for each section are shown in Table I.

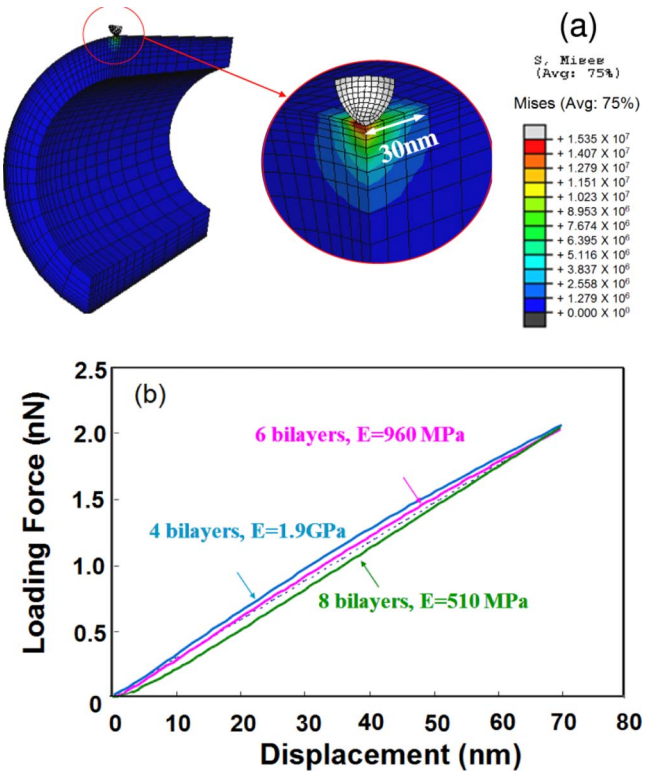

FIG. 5. (Color online) (a) Simulated deformation of the half segment of a modeled tubule with an external radius of 266 nm, corresponding to the section 2 shown in Fig. 4(a). The distribution of the von Mises stress coded by color is clearly seen in the zooming image at the contact point. (b) Simulated force-displacement curves (solid lines) of the modulated tubule. During the simulation, the external radius of the tubule was kept constant, while the number of bilayers in the tubule wall was varied. The Young's modulus E was chosen such that the simulated curve (solid lines) within 70 nm displacement could be best fitted with the measured spring constant of 0.039 N/m (dashed line). The optimized fitting results are four bilayers, E=1.9 GPa, six bilayers, E=960 MPa, and eight bilayers, E=510 MPa.

The morphology of the cigarlike tubule can be characterized by the t/R_{ext} (relative wall thickness). In the regime $0.11 < t/R_{ext} < 0.23$, we find that the E is very sensitive to the t/R_{ext}. As can be seen from Fig. 6(a), the E decreases rapidly for the t/R_{ext} smaller than 0.19 and slightly decreases for the

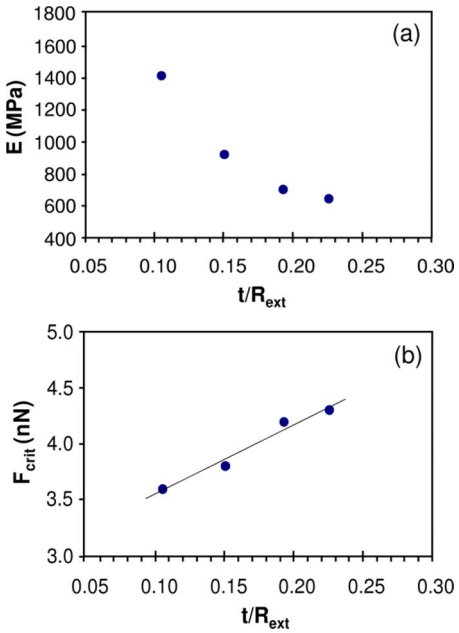

FIG. 6. (Color online) (a) The calculated E of lipid tubules as a function of the wall thickness/external radius (t/R_{ext}). (b) The measured critical buckling force F_{crit} of lipid tubules as a function of the t/R_{ext}. The F_{crit} was measured from the first forward FZ curve of each section of the tubule shown in Fig. 4(a).

t/R_{ext} between 0.19 and 0.23. The origin of the high E of the tubules with low t/R_{ext} might be a result of surface effects. In general, the influence of surface effects on the mechanical properties of materials becomes relevant at the nanoscale. For example, the Young's modulus of multiwalled carbon nanotubes was found to increase significantly with decreasing diameters [49]. The moduli of silver and lead nanowires with smaller diameter were found to be higher than that of the larger ones [50]. For polypyrrole tubes, the surface effect on their modulus was found to be more pronounced [51]. These size-dependent mechanical behaviors are believed to be a surface-stiffening effect which dominates at large surface-to-volume ratio.

The F_{crit} shown in Table I was measured from the first forward FZ curve of each section of the cigarlike tubule in Fig. 4(a). Interestingly, we find that the F_{crit} linearly scales as the relative wall thickness t/R_{ext} [Fig. 6(b)]. Studies have shown that the main factor determining the buckling of spherical shells by capillary force is the t/R_{ext} ratio [52]. This can be understood by elastic theory, which predicts that the force needed to buckle a spherical shell scales as $(t/R_{ext})^2$ [53]. In our experiments, buckling of lipid tubules is induced by a point force. We show that F_{crit} scales as t/R_{ext} rather than $(t/R_{ext})^2$. The nonzero intercept with the F_{crit} axis might be due to the surface-tension contribution.

To optimize lipid tubules for technological applications, a great effort has been made in manipulating the morphology of lipid tubules, including radius and wall thickness [54–57]. Control of radius is critical because it determines the release rate in tubule-based release systems. Control of wall thickness is important because the thickness determines whether the tubules can sustain metallization. Therefore, a better understanding of how the morphology of lipid tubules affects their mechanical properties may provide a framework for optimizing lipid tubules for technological applications.

In summary, buckling or failure of lipid tubules is expected when the stress exceeds their ultimate strengths. To probe the mechanical strength of lipid tubules, we examine the limit of the elastic response of lipid tubules under AFM indentations by increasing loading forces. The discontinuity in the FZ curves, which is a result of the buckling transition of lipid tubules, is observed when the loading force exceeds a critical force. The buckled lipid tubules can slowly regain their origin convex curvature after relaxation in water at room temperature. The critical force at which lipid tubules undergo the buckling transition from convex to concave curvature is found to scale linearly as t/R_{ext}. Furthermore, we find that the critical buckling force decreases near the ends of lipid tubules.

ACKNOWLEDGMENT

This work was supported by the National Science Foundation (Contract No. CMMI 0726478).

[1] E. M. Wilson-Kubalek, R. E. Brown, H. Celia, and R. A. Milligan, Proc. Natl. Acad. Sci. U.S.A. **95**, 8040 (1998).
[2] Z. X. Zhang, T. J. Melia, F. He, C. Yuan, A. McGough, M. F. Schmid, and T. G. Wensel, J. Biol. Chem. **279**, 33937 (2004).
[3] A. J. Patil, E. Muthusamy, A. M. Seddon, and S. Mann, Adv. Mater. (Weinheim, Ger.) **15**, 1816 (2003).
[4] R. R. Price, W. J. Dressick, and A. Singh, J. Am. Chem. Soc. **125**, 11259 (2003).
[5] J. H. Jung, S. H. Lee, J. S. Yoo, K. Yoshida, T. Shimizu, and S. Shinkai, Chem.-Eur. J. **9**, 5307 (2003).
[6] Y. Zhao, J. Liu, Y. Sohn, and J. Y. Fang, J. Phys. Chem. C **111**, 6418 (2007).
[7] T. Delclos, C. Aime, E. Pouget, A. Brizard, I. Huc, M. H. Delville, and R. Oda, Nano Lett. **8**, 1929 (2008).
[8] J. M. Schnur, R. Price, and A. S. Rudolph, J. Controlled Release **28**, 3 (1994).
[9] N. J. Meilander, M. K. Pasumarthy, T. H. Kowalczyk, M. J. Cooper, and R. V. Bellamkonda, J. Controlled Release **88**, 321 (2003).
[10] N. Kameta, H. Minamikawa, M. Masuda, G. Mizuno, and T. Shimizu, Soft Matter **4**, 1681 (2008).
[11] N. Kameta, M. Masuda, H. Minamikawa, N. V. Goutev, J. A. Rim, J. H. Jung, and T. Shimizu, Adv. Mater. (Weinheim, Ger.) **17**, 2732 (2005).
[12] L. T. Yu, I. A. Banerjee, X. Y. Gao, N. Nuraje, and H. Matsui, Bioconjugate Chem. **16**, 1484 (2005).
[13] Y. Zhao, N. Mahajan, and J. Y. Fang, Small **2**, 364 (2006).
[14] N. Kameta, M. Masuda, G. Mizuno, N. Morii, and T. Shimizu, Small **4**, 561 (2008).
[15] M. Caffrey, J. Hogan, and A. S. Rudolph, Biochemistry **30**, 2134 (1991).
[16] J. M. Schnur, B. R. Ratna, J. V. Selinger, A. Singh, G. Jyothi, and K. R. K. Easwaran, Science **264**, 945 (1994).
[17] B. N. Thomas, C. R. Safinya, R. J. Plano, and N. A. Clark, Science **267**, 1635 (1995).
[18] U. Lauf, A. Fahr, K. Westesen, and A. S. Ulrich, ChemPhysChem **5**, 1246 (2004).
[19] Y. Zhao, N. Mahajan, R. Lu, and J. Y. Fang, Proc. Natl. Acad. Sci. U.S.A. **102**, 7438 (2005).
[20] N. Mahajan, Y. Zhao, D. Du, and J. Y. Fang, Langmuir **22**, 1973 (2006).
[21] A. Brizard, C. Aime, T. Labrot, I. Huc, D. Berthier, F. Artzner, B. Desbat, and R. Oda, J. Am. Chem. Soc. **129**, 3754 (2007).
[22] P. Nelson and T. Powers, Phys. Rev. Lett. **69**, 3409 (1992).
[23] S. Komura and O. Y. Zhong-can, Phys. Rev. Lett. **81**, 473 (1998).
[24] J. V. Selinger, M. S. Spector, and J. M. Schnur, J. Phys. Chem. B **105**, 7157 (2001).
[25] R. L. B. Selinger, J. V. Selinger, A. P. Malanoski, and J. M. Schnur, Phys. Rev. Lett. **93**, 158103 (2004).
[26] Z. C. Tu and U. Seifert, Phys. Rev. E **76**, 031603 (2007).
[27] H. Frusawa, A. Fukagawa, Y. Ikeda, J. A. Araki, K. Ito, G. John, and T. Shimizu, Angew. Chem., Int. Ed. **42**, 72 (2003).
[28] Y. Zhao, L. An, and J. Y. Fang, Nano Lett. **7**, 1360 (2007).
[29] Y. Zhao and J. Y. Fang, J. Phys. Chem. B **112**, 10964 (2008).
[30] D. E. Laney, R. A. Garcia, S. M. Parsons, and H. G. Hansma,

Biophys. J. **72**, 806 (1997).
[31] N. Delorme and A. Fery, Phys. Rev. E **74**, 030901(R) (2006).
[32] W. S. Klug, R. F. Bruinsma, J. P. Michel, C. M. Knobler, I. L. Ivanovska, C. F. Schmidt, and G. J. L. Wuite, Phys. Rev. Lett. **97**, 228101 (2006).
[33] C. Carrasco, A. Carreira, I. A. T. Schaap, P. A. Serena, J. Gomez-Herrero, M. G. Mateu, and P. J. de Pablo, Proc. Natl. Acad. Sci. U.S.A. **103**, 13706 (2006).
[34] N. Kol, M. Gladnikoff, D. Barlam, R. Z. Shneck, A. Rein, and I. Rousso, Biophys. J. **91**, 767 (2006).
[35] Y. Zhao, Z. Ge, and J. Y. Fang, Phys. Rev. E **78**, 031914 (2008).
[36] P. J. de Pablo, I. A. T. Schaap, F. C. MacKintosh, and C. F. Schmidt, Phys. Rev. Lett. **91**, 098101 (2003).
[37] A. Kis, S. Kasas, B. Babić, A. J. Kulik, W. Benoit, G. A. D. Briggs, C. Schönenberger, S. Catsicas, and L. Forró, Phys. Rev. Lett. **89**, 248101 (2002).
[38] N. Kol, L. Adler-Abramovich, D. Barlam, R. Z. Shneck, E. Gazit, and I. Rousso, Nano Lett. **5**, 1343 (2005).
[39] J. F. Graveland-Bikker, I. A. T. Schaap, C. F. Schmidt, and C. G. de Kruif, Nano Lett. **6**, 616 (2006).
[40] K. M. Munson, P. G. Mulugeta, and Z. J. Donhauser, J. Phys. Chem. B **111**, 5053 (2007).
[41] J. F. Smith, T. P. J. Knowles, C. M. Dobson, C. E. MacPhee, and M. E. Welland, Proc. Natl. Acad. Sci. U.S.A. **103**, 15806 (2006).
[42] Y. Zhao, K. Tamhane, X. Zhang, L. An, and J. Y. Fang, ACS Nano **2**, 1466 (2008).
[43] P. Yager and P. E. Schoen, Mol. Cryst. Liq. Cryst. **106**, 371 (1984).
[44] I. L. Ivanovska, P. J. de Pablo, B. Ibarra, G. Sgalari, F. C. Mackintosh, J. L. Carrascosa, C. F. Schmidt, and G. J. L. Wuite, Proc. Natl. Acad. Sci. U.S.A. **101**, 7600 (2004).
[45] J. P. Michel, I. L. Ivanovska, M. M. Gibbons, W. S. Klug, C. M. Knobler, G. J. L. Wuite, and C. F. Schmidt, Proc. Natl. Acad. Sci. U.S.A. **103**, 6184 (2006).
[46] C. R. Calladine, *Theory of Shell Structures* (Cambridge University Press, New York, 1983).
[47] L. Guo, P. Chowdhury, J. Y. Fang, and F. Gai, J. Phys. Chem. B **111**, 14244 (2007).
[48] J. L. Hutter and J. Bechhoefer, Rev. Sci. Instrum. **64**, 3342 (1993).
[49] I. Palaci, S. Fedrigo, H. Brune, C. Klinke, M. Chen, and E. Riedo, Phys. Rev. Lett. **94**, 175502 (2005).
[50] S. Cuenot, C. Fretigny, S. Demoustier-Champagne, and B. Nysten, Phys. Rev. B **69**, 165410 (2004).
[51] S. Cuenot, C. Fretigny, S. Demoustier-Champagne, and B. Nysten, Phys. Rev. Lett. **85**, 1690 (2000).
[52] C. I. Zoldesi, I. L. Ivanovska, C. Quilliet, C. J. L. Wuite, and A. Imhof, Phys. Rev. E **78**, 051401 (2008).
[53] L. Landau and E. Lifshitz, *Course of Theoretical Physics, Vol. 7*, Theory of Elasticity (Butterworth-Heinemann, Oxford, 1997).
[54] M. S. Spector, J. V. Selinger, A. Singh, J. M. Rodriguez, R. R. Price, and J. M. Schnur, Langmuir **14**, 3493 (1998).
[55] M. S. Spector, A. Singh, P. B. Messersmith, and J. M. Schnur, Nano Lett. **1**, 375 (2001).
[56] M. Masuda and T. Shimizu, Langmuir **20**, 5969 (2004).
[57] J. P. Douliez, B. Pontoire, and C. Gaillard, ChemPhysChem **7**, 2071 (2006).